Silicon (2023) 15:4795–4809
https://doi.org/10.1007/s12633-023-02389-4

ORIGINAL PAPER

Elastic Properties of Randomly Dispersed Functionalized Silicon Carbide Nanotubes/Polymer Nanocomposites: Combined Multiscale Molecular Dynamics and Finite Element Modeling

M. Eghbalian[1] · R. Ansari[2] · S. Haghighi[1]

Received: 6 December 2022 / Accepted: 3 March 2023 / Published online: 14 March 2023

Abstract
A molecular dynamics (MD)-finite element (FE) modeling scheme is proposed to study the effective Young's modulus of polymer nanocomposites reinforced by functionalized silicon carbide nanotubes (fSiCNTs). By evaluating the tensile and shear properties of the polymer matrix strengthened by hydroxyl (O–H)-, fluorine (F)-, and hydrogen (H)-fSiCNTs (O-, F-, and H-fSiCNT/polymer) through MD simulations, FE modeling with the consideration of equivalent solid fibers (ESFs) is conducted and the ratio of effective Young's modulus of the unit cell (E_{UC}) to Young's modulus of the polymer matrix (E_P) is reported. The influence of the chirality, and chemical functionalization of nanotubes along with the effects of the volume fraction of the ESFs, and polymer materials on the E_{UC} are discovered. The results show that the random dispersion of ESFs containing armchair fSiCNTs (ESFs-armchair fSiCNTs) within the polymers (ESFs-armchair fSiCNTs/polymer) instead of the ESFs-pure armchair fSiCNTs leads to reducing the E_{UC}. In every ESFs volume fraction (ν_f), the reinforcement impact of the ESFs-armchair and zigzag fSiCNTs on the polyethylene (PE) is more significant in comparison with the polypropylene (PP). Using the ESFs-zigzag H- and F-fSiCNTs/PP instead of the ESFs-pure zigzag SiCNTs/PP decreases $^{E_{UC}}/_{E_P}$, while at the ESFs' ν_f over 10%, the $^{E_{UC}}/_{E_P}$ of the ESFs-zigzag O-fSiCNTs/PP is higher than that of the ESFs-pure zigzag SiCNTs/PP. The ESFs-zigzag H- and F-fSiCNTs/PE as compared to the ESFs-pure zigzag SiCNTs/PE are experienced larger effective elastic moduli, however, only at the ESFs' ν_f of 50%, the reinforcing impact of the ESFs-zigzag O-fSiCNTs within the PE is more considerable than that of the ESFs-pure zigzag SiCNTs.

Keywords Silicon carbide nanotube · Effective Young's modulus · Covalent functionalization · Molecular dynamics simulation · Finite element method

1 Introduction

The most widely used advanced composites, polymer matrix composites (PMCs), are characterized based on three components called matrix phase, reinforcement, and the interfacial region between matrix and reinforcement. A matrix is a continuous phase of composites and it can have macro- or micro-dimensions [1–5]. Unlike metals and ceramics matrices, easy processing conditions, low cost, and mechanical flexibility of polymers offer substantial benefits to meet engineering requirements [6–9]. Due to the more desirable characteristics of PMCs compared to conventional metals or unreinforced polymers, general demand for PMCs has been increasing worldwide. The PMCs are considerably excellent in both fatigue and corrosion resistance in comparison with metals [10]. Furthermore, the PMCs weigh less than conventional polymers and possess high strength and stiffness along the direction of the reinforcement. To fulfill the need of a specific application, the PMCs' form and features can be tailored which makes them more attractive. That is why the PMCs have found a vast variety of applications in automobiles, aircraft, electronics, biomedical instruments,

✉ M. Eghbalian
meghbalianarani@gmail.com

✉ R. Ansari
r_ansari@guilan.ac.ir

[1] Faculty of Mechanical Engineering, University Campus 2, University of Guilan, Rasht, Iran

[2] Faculty of Mechanical Engineering, University of Guilan, P.O. Box 3756, Rasht, Iran

consumer products, and construction products, to mention a few [2, 11]. The PMCs are categorized into two groups namely thermoplastic or thermoset matrix resins reinforced by organic or inorganic fibers. Amongst thermoplastics polymers (e.g., polypropylene (PP), polyethylene (PE), polymethyl methacrylate (PMMA), polyvinyl chloride (PVC), Nylon), ethylene- and propylene-based polyolefins have been gaining in popularity [12]. Polyolefins composites are stronger than thermosets polymeric (e.g., epoxy, polyimide, polyester resins) systems with the contribution of their semicrystalline and amorphous configurations [2]. Regarding the discontinuous phase of composites, i.e., reinforcements, they commonly exist in the micro- or nano-scale.The fundamental aim of intercalating the reinforcement into the matrix is to enlarge energy absorption and take advantage of their great stiffness and strength. [1]. Silicon carbide (SiC)-based materials have been highly recommended to be used as reinforcement phases of composites because of their remarkable ability to work in harsh environments and their usage in high-voltage, high-temperature, and high-power electronic switches and rectifiers [13, 14]. The SiC exhibits semiconducting properties in the bulk form and it is recognized as a wide-bandgap semiconductor with ultra-high strength, high thermal conductivity, low thermal expansion, and good thermal stability [15, 16]. In addition to these charming properties of bulk SiC in macroscale, the quantum-size effects of SiC nanostructures prompt outstanding physicochemical features [17, 18]. Accordingly, nanostructures made of SiC have been extensively utilized in nanosensors for hazardous gases detection, optoelectronic devices, gas seal rings in compressor pumps, capsule materials for nuclear equipment, and biomedical engineering [19–21]. As the technology of crystal growth advances, the structures based on the SiC have been serving as building blocks for nanoscale electronics. As well as that the SiC nanostructures are reported to have enormous potential to use in nanocomposites because of their extremely high fracture strength [22–24]. Of 1D SiC nanosystems, the advantages of silicon carbide nanotubes (SiCNTs) outweigh their nanowires counterparts owing to having hollow configurations. Also, the SiCNTs are durable under elevated temperatures and reveal high melting temperatures. These nanotubes can retain their stability under 1000 °C (in air) [25, 26]. Compared to the carbon nanotubes (CNTs), the SiCNTs have drawn attention due to the capability of storing more hydrogen, less toxic impact while interacting with living cells, higher solubility, and comfier sidewall functionalization [20, 27, 28]. All the aforementioned characteristics make the SiCNTs absolutely ideal for working in extreme environments and conditions that cannot be guaranteed by employing CNTs. What is more, from both theoretical (e.g., density functional theory (DFT)) and experimental perspectives, the existence of tubular and graphitic forms of SiC has been anticipated [29–32]. Besides, multiple strategies have been reported to perform the prosperous synthesis of the SiCNTs such as the method of extreme hole injection, and high-temperature reactions between Si powders and CNTs at 1200 °C for 100 h [29, 31]. Despite conducted experimental studies to measure properties of SiC-based nanocomposites, extensive theoretical research has been performed by computer simulation techniques to elucidate the experimental measurements and to circumvent technical challenges of the real experiments at the nanoscale. Molecular dynamics (MD) simulations and finite element (FE) based multiscale modeling are quite popular for theoretically studying the elastic properties of nanocomposites [33–38]. However, MD simulations of nanocomposites tend to be very time-consuming and be inappropriate for structures with the complexity of dimensions because of which these models have often contained merely a single nanofiller in the matrix that is tuned in a defined direction. This is in contrast to real nanocomposite materials that include several reinforcements with a wide diversity of arbitrary distributions and orientations [39, 40]. Consequently, the FE analysis can be perfectly effective in having more realistic modeling of randomly dispersed reinforcement/polymer nanocomposites with a longer time. In this regard, the FE techniques have been widely used to investigate the random dispersion of CNTs within polymer matrices [41–47]. Hence, this paper aims at finding effective Young's modulus of the equivalent solid fibers (ESFs) containing functionalized silicon carbide nanotubes (fSiCNTs) within the polymers (ESFs-fSiCNTs/polymer) and ESFs containing pure silicon carbide nanotubes (SiCNTs) within the polymers (ESFs-pure SiCNTs/polymer) nanocomposites through a two-step modeling scheme. To achieve this perpose, MD simulations in conjunction with FE approach are employed. In the first step, with the consideration of the impact of the interfacial region, an MD-based cubic representative volume element (RVE) containing the fSiCNT and polymer matrix is simulated to calculate the longitudinal and transverse tensile features and shear properties of the system as well. Next, the FE modeling is performed and MD results are fed to FE models to account for Young's modulus of the unit cell (E_{UC}) of the ESFs-fSiCNTs/polymer. The effects of different volume fractions of ESFs, nanotubes' chirality (zigzag and armchair), various functional atoms (O, F, H), and polymer materials (PE and PP) on the E_{UC} are explored. Moreover, it is important to recall that the prediction of the mechanical properties is considered to be absolutely indispensable for the design and application of polymeric nanocomposite materials strengthened by SiCNTs. The underlying reasons stem from the fact that lattice or thermal mismatch between nanoscale materials may lead to acute

stresses especially when SiC-based nanoelectromechanical systems (NEMS) are subjected to external loadings, being operated in harsh environments [13].

2 Methodology

2.1 Molecular Dynamics Method

To begin with, the MD simulations are performed to compute five independent elastic properties of the transversely isotropic RVEs of the fSiCNTs/ and pure SiCNTs/polymer. These five independent characteristics (longitudinal Young's modulus ($(E_L)E_x$), transverse Young's modulus ($(E_T)E_y$), shear modulus in XY plane (G_{xy}), shear modulus in YZ plane (G_{yz}), Poisson's ratio (ϑ_{xy})) are utilized to create the stiffness matrix (C_{ij}) which is supposed to be used as input to the FE modeling. The C_{ij} for transversely isotropic nanocomposites can be expressed by [48]:

$$C_{ij} = \begin{bmatrix} C_{11} & C_{12} & C_{12} & 0 & 0 & 0 \\ C_{12} & C_{22} & C_{23} & 0 & 0 & 0 \\ C_{12} & C_{23} & C_{22} & 0 & 0 & 0 \\ 0 & 0 & 0 & \frac{C_{22}-C_{23}}{2} & 0 & 0 \\ 0 & 0 & 0 & 0 & C_{66} & 0 \\ 0 & 0 & 0 & 0 & 0 & C_{66} \end{bmatrix}, \; C_{ij} = C_{ji} \tag{1}$$

In which ($C_{11}, C_{12}, C_{22}, C_{23}, C_{66}$) represent five independent elastic constants. In this work, Large-scale Atomic/Molecular Massively Parallel Simulator (LAMMPS) code is employed to conduct tensile tests (longitudinal and perpendicular tensions) and shear tests (shearing in XY and YZ planes) for each prepared model. To define inter-and intra-molecular interactions and determine the potential energy between atoms, generic Dreiding force field [49] and Tersoff potential function are considered [50]. Tersoff potential function calculates the energy terms among C and Si atoms in the SiCNT whereas interactions in the polymers, the place of functionalization, and between the nanotubes and polymer chains are modeled by generic Dreiding force field and Lennard–Jones (L-J) potential. Periodic boundary conditions are imposed on all x, y, z directions of the cubic RVE structure. Choosing a time step of 0.5 fs, Newton equations are integrated according to Velocity-Verlet algorithm to describe the time-dependent behavior of a classical molecular system [51, 52]. After initial energy minimization by using the conjugate gradients technique, a canonical ensemble (NVT) simulation is implemented for 500 ps at 300 K. Following this stage, two further ensemble simulations are accomplished to achieve an equilibrated, geometry-optimized configuration. During these three equilibration processes, the thermodynamic properties (temperature and pressure) of the system are controlled by Nosé-Hoover method [53]. The first step is followed by 0.5 ns of isothermal-isobaric (NPT) ensemble simulation at 300 K and 1 bar. Subsequently, the RVE is put into another NVT ensemble for 300 ps to relax at room temperature. Then, the uniaxial tension tests are simulated by applying a displacement of 0.000025 Å to each boundary of the equilibrated RVE along three loading directions (the X, Y, Z axes) separately. Periodic boundary conditions are selected for directions perpendicular to the applied strain whereas a shrink-wrapped, and non-periodic boundary condition is employed along the loading direction. The system is stretched till the external strain is elevated up to 5% and bond-breaking happens. Also, the outcomes are stored at every 1000 times steps. Finally, the slope of the stress–strain profiles is calculated to measure longitudinal and transverse Young's moduli (E_x and E_y). To perform the shear tests in the XY, and YZ planes, the equilibrated RVE is distorted at each time step, and the component of stress in the loading direction is determined within the elastic limit. By using the shear stress-shear strain relation known as Hooke's law in shear, shear moduli in the XY, and XZ planes (G_{xy}=G_{yx} =G_{xz}=G_{zx}) and shear modulus in the YZ plane (G_{yz}=G_{zy}) are estimated. Then, the fifth independent elastic constant of the stiffness matrix (ϑ_{xy}) is obtained by computing the ratio of the mean of transverse strain to the imposed normal strain. To this end, the pressure in the loading direction is not controlled to keep the external strain whereas the pressure tensor normal to the loading direction is allowed to be held at 1 atm. The generated results showed good agreement with the existing work in the open literature [39, 54]. Eventually, with the calculation of all independent and dependent elastic features, the C_{ij} of transversely isotropic fSiCNT/polymer nanocomposite is determined. It is worth noting that due to simple relations of the inverse of stiffness matrix (compliance matrix) with the elastic moduli and Poisson's ratios, the compliance matrix (S_{ij}) tends to be computed. The relationship between S_{ij} and C_{ij} is given by the following equation [55, 56]:

$$C_{ij} = S_{ij}^{-1} = \begin{bmatrix} \frac{1}{E_x} & \frac{-\vartheta_{xy}}{E_x} & \frac{-\vartheta_{xy}}{E_x} & 0 & 0 & 0 \\ \frac{-\vartheta_{xy}}{E_x} & \frac{1}{E_y} & \frac{-\vartheta_{yz}}{E_y} & 0 & 0 & 0 \\ \frac{-\vartheta_{xy}}{E_x} & \frac{-\vartheta_{yz}}{E_y} & \frac{1}{E_y} & 0 & 0 & 0 \\ 0 & 0 & 0 & \frac{2(1+\vartheta_{yz})}{E_y} & 0 & 0 \\ 0 & 0 & 0 & 0 & \frac{1}{G_{xy}} & 0 \\ 0 & 0 & 0 & 0 & 0 & \frac{1}{G_{xy}} \end{bmatrix}^{-1} \tag{2}$$

Where ϑ_{yz} is defined as:

$$\frac{1}{G_{yz}} = \frac{2(1+\vartheta_{yz})}{E_y} \rightarrow \vartheta_{yz} = \frac{E_y}{2\,G_{yz}} - 1 \tag{3}$$

2.2 Molecular Dynamics Models

First off, the (11,0) zigzag and (6,6) armchair-types SiCNT and fSiCNTs as reinforcements are modeled by using MATLAB software. The length of the armchair and zigzag

SiCNTs is considered ~ 68.1 Å and ~ 73.2 Å, respectively. The choice of these geometrical and structural characteristics makes it possible for us to compare the results. As to the functionalized reinforcements (fSiCNTs), three functional agents namely H, F, and O atoms are covalently connected to the SiCNTs' wall to investigate the functionalization effect. It should be noted that rather than atomic O, the hydroxyl group (O–H) is attached to the host structure and the O-fSiCNT refers to the configuration that is chemically functionalized by O–H. The linkage of foreign atoms to the host structure is performed based on the random distribution pattern. To diminish the impact of functionalized spots on the results, three varied states of the random pattern are considered. Accordingly, each nanotube is modeled three times in every functionalization degree, and the ultimate quantity of tensile properties is obtained from averaging three cases. Furthermore, the weight percentage of randomly distributed atoms is selected 10%. Regarding polymer matrices, Accelrys Materials Studio software is employed to simulate the initial structure of PE and PP chains each of which comprises 15 monomers. Figure 1 is provided to display the initial structure of the reinforcements, i.e., SiCNT and fSiCNTs. Similarly, a sample of the primary molecular structure of the PP matrix along with repeating units of PE and PP chains can be observed in Fig. 2. It is worth noting further details about these chosen functional groups, reinforcements, and polymer matrices can be found in our newly published work [13, 16, 21]. Having been simulated nanofillers and polymers, Packmol software package is utilized to model the RVE configuration of SiCNTs/polymer and fSiCNT/polymer [57]. The primary density of the RVE is considered 1.05 $^{gr}/_{cm^3}$, and the volume fraction of nanofiller is accounted for ~ 10%. This way, the dimensions of RVE periodic boxes for (6,6) fSiCNT/polymer, and (11,0) fSiCNT/polymer are estimated $33.61 \times 33.61 \times 68.06$ Å^3, $35.29 \times 35.29 \times 73.23$ Å^3, correspondingly. Some examples of molecular structures of the fSiCNTs/polymer RVEs are depicted in Fig. 3.

2.3 Details of Finite Element Modeling

To compute effective Young's modulus of polymer nanocomposites strengthened by ESFs-fSiCNTs (ESFs-fSiCNTs/polymer) via the FE analysis, the ABAQUS software is chosen. First of all, the initial geometrical structure of each part, i.e., ESFs and polymer, is simulated separately and the cross-sectional area of each part is regarded as a homogeneous solid. Next, two different parts of the unit cell (ESFs and polymeric solid cube) are merged to form the unit cell comprising randomly distributed ESFs. To achieve this, the MD-based cubic RVE is turned into a homogenized cubic ESF (C-ESF) which demonstrates the transversely isotropic

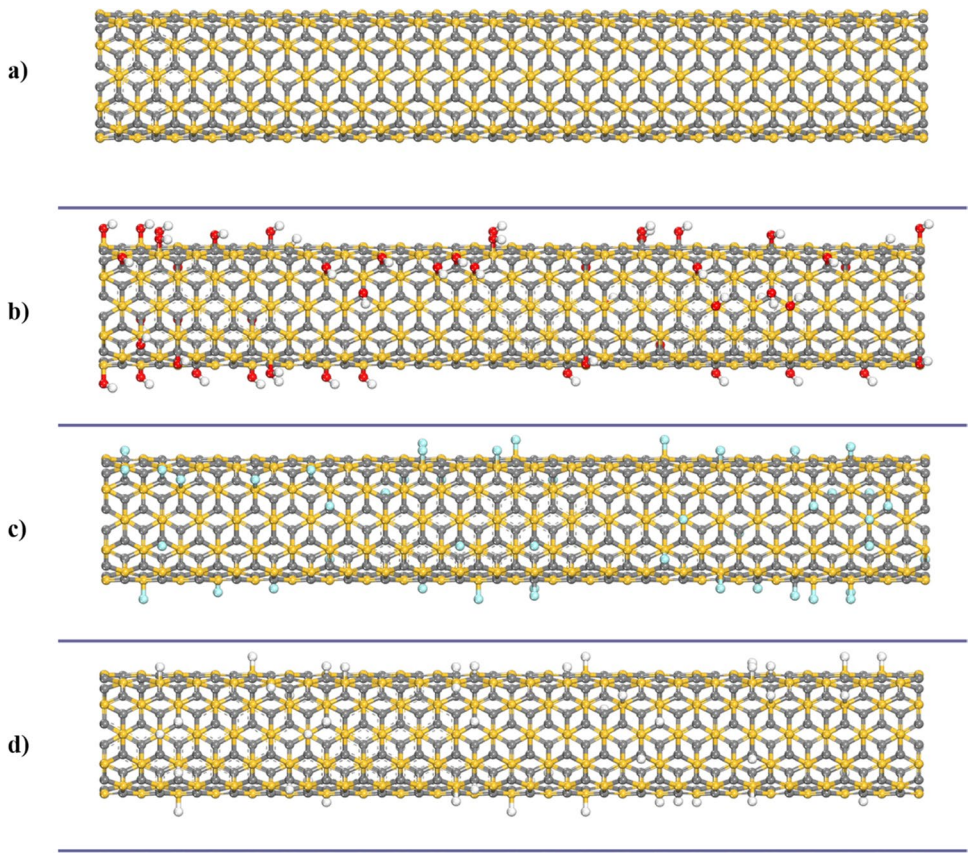

Fig. 1 Schematic representation of **a** SiCNTs, **b** O-fSiCNT, **c** F-fSiCNT, **d** H-fSiCNT

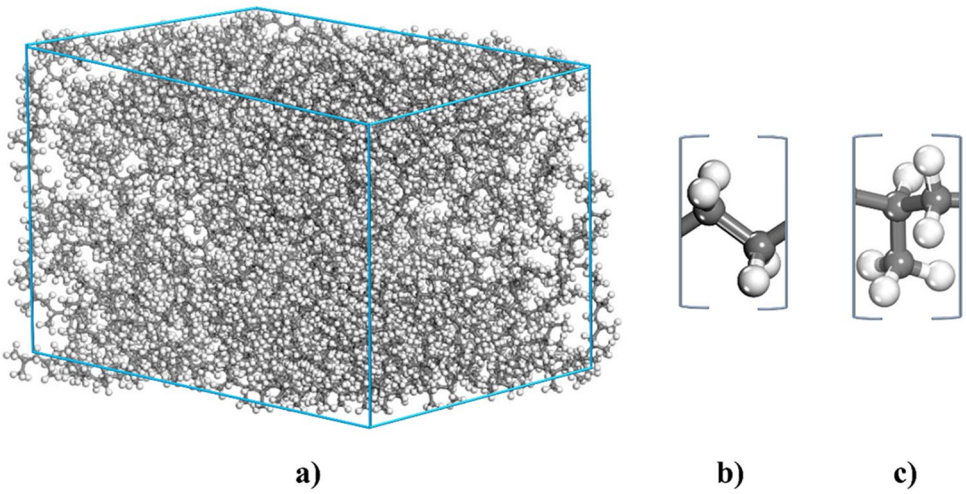

Fig. 2 **a** Molecular structure of the PP matrix, **b** repeating unit for the PE, **c** repeating unit for the PP

behavior. As the properties of the C-ESF are independent of the RVE dimensions and shape, these characteristics can be used in new geometrical structures whose dimensions are the same as the C-ESF. To this end, the current C-ESF is transformed into a cylindrical structure whose length and cross-sectional area are almost equal to the length and cross-section of the C-ESF. This cylindrical configuration is so-called the ESF. Not only does this equivalence assist in not getting involved in the FE modeling of the interface region, but also it allows us to make easier comparisons with FE-based previous studies which were directly dealt with the random dispersion of nanotubes in the polymer matrix. This equivalence is shown in Fig. 4. In the FE modeling, the basic point is that the volume fraction (ν_f) of ESFs inside the polymer matrices needs to be accurately determined. In the earlier section, the ν_f of nanotubes within the RVE is evaluated to be 10% ($\nu_{f_{NT}} = 10\%$) which implies that the nanotubes include 10% of each ESF's volume. Therefore, the total volume fraction of nanotubes in the FE-based unit cell (ν_{f_T}) can be obtained as

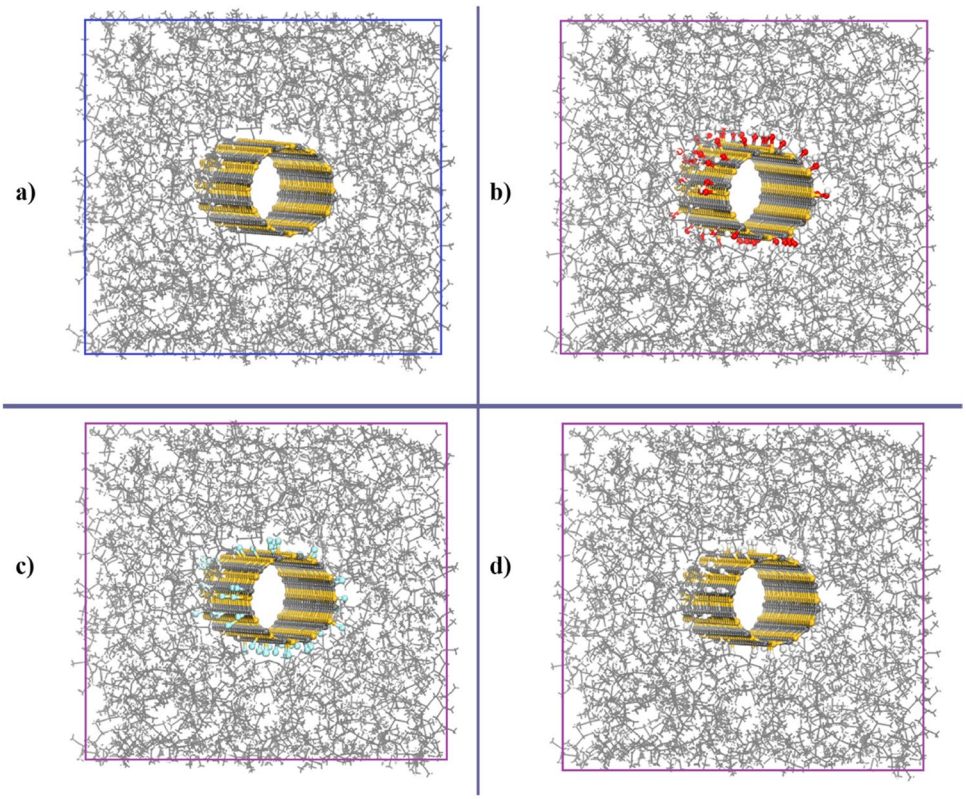

Fig. 3 MD-based RVE model of **a** SiCNT/PP, **b** O-fSiCNT/PP, **c** F-fSiCNT/PP, **d** H-fSiCNT/PP

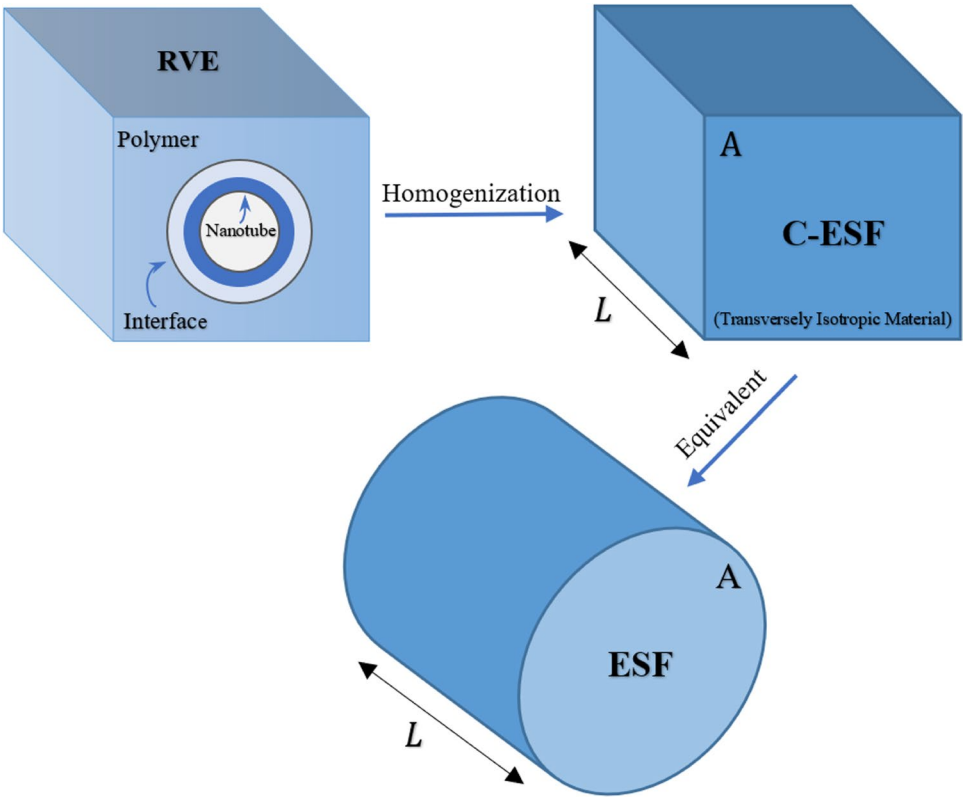

Fig. 4 Schematic view of converting the MD-based RVE into the FE model of the ESF

$$\nu_{f_T} = \nu_{f_{NT}} \times \nu_{f_{ESF}} \tag{4}$$

Where $\nu_{f_{NT}}$, and $\nu_{f_{ESF}}$ denote the volume fraction of nanotubes in the MD-based cubic RVE, and volume fraction of ESFs inside the polymers in the FE-based unit cell, respectively. In this paper, the ν_{f_T} is assumed to be 1%, 3%, and 5% which means that the ESFs constitute 10%, 30%, and 50% of the volume of the FE-based unit cell, correspondingly. Accordingly, the 15, 45, and 75 ESFs are randomly distributed in the PE and PP matrices (see Fig. 5). In addition to the modeled ESFs, a sample of the ESFs-nanotubes/polymer unit cell is revealed in Fig. 5. To compare the outcomes, the volume of ESFs including armchair and zigzag nanotubes is selected nearly equal. Thus, the unit cell with the same dimensions in both cases is generated. Each side length of the cubic unit cell is considered ~ 500 Å. The size of unit cells and geometrical characteristics of fillers (ESFs and nanotubes) are summarized in Table 1. In this paper, the ESFs are modeled as transversely isotropic materials while the polymers are considered as isotropic materials whose mechanical properties, i.e., Young's modulus and a Poisson's ratio, are obtained from MD simulations. Also, the C_{ij} is introduced to the software (see Eq. 1) as the mechanical feature of the ESFs. It should be noted that the unit of all fed Young's moduli to ABAQUS software is defined as N/Å^2 to have a precise dimensional simulation at the nanolevel. Eventually, the simulated parts are combined and the interactions between the polymers and the ESFs are assumed to be a perfect bonding. The fact is that despite several approximate methods reported on FE modeling of the interfacial region, the use of these approaches is restricted due to the facing challenges in the simulation of the complicated nature of the interface. Therefore, the utilization of ESFs can overcome those obstacles because the ESFs are representative of MD-based RVE and the interfacial effect has already been considered. Moreover, to calculate the effective elastic modulus, it is necessary to apply displacement over different sides in the unit cell. Having been fixed a reference point on a plane, this displacement (~ 25 Å) is imposed on the reference point at the intersection of the diameters of each side. Then it is coupled with various parts of that plane. This causes a uniform displacement of each side of the unit cell. Each loading to the reference point is individually conducted along x, y, and z directions and the average of three cases is reported as the final outcome. The clamped-free boundary condition is assumed based on which the unit cell side in front of the plane on which the strain is imposed, needs to be fixed while other sides are completely free. Another point that should be mentioned is that quadratic tetrahedral elements (C3D10) are chosen to measure the effective Young's modulus of the unit cell. These elements are capable of analyzing three-dimensional stress and the specimens are meshed by using tetragonal shape elements. The optimal value of ~ 20 Å is obtained for the mesh-seed length. To discover this optimal value, the unit cell meshes in three different seed sizes and Young's modulus

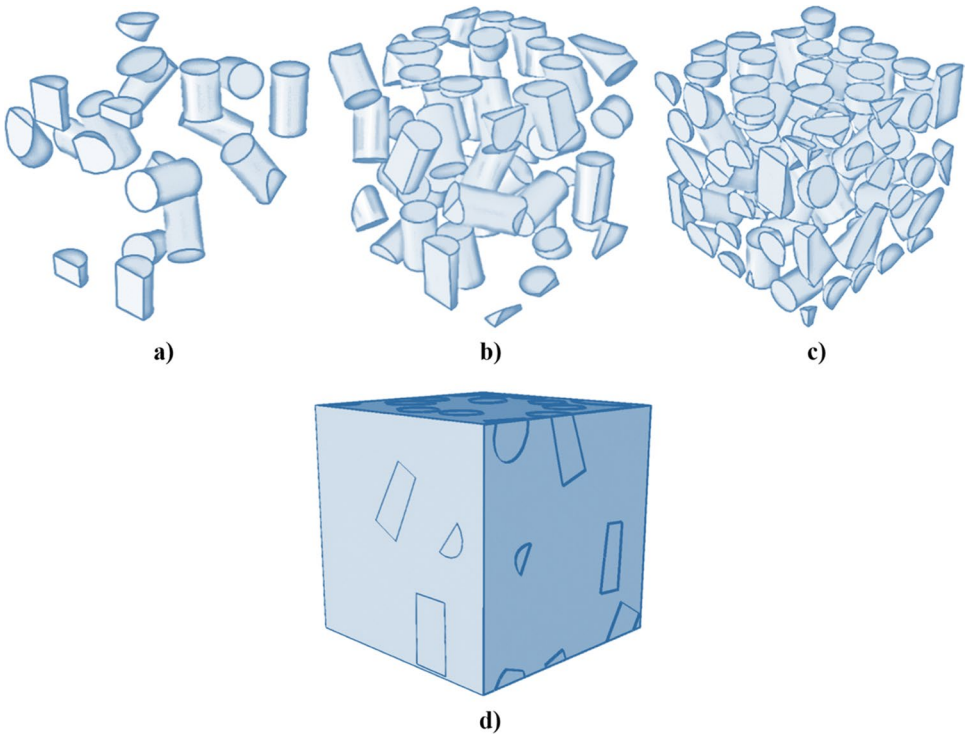

Fig. 5 FE model of **a** 15 ESFs, **b** 45 ESFs, **c** 75 ESFs, **d** ESFs-SiCNTs/polymer unit cell

of the meshed unit cells is computed. The findings are experienced the lowest dependence on the size of elements at mesh seed size of ~ 20 Å. A sample of the meshed unit cell and its components is illustrated in Fig. 6. This unit cell can represent a bulk composite material. Additionally, according to Hooke's law, the effective Young's modulus of the ESFs-SiCNTs/polymer nanocomposite within the linear elastic limit of stress/strain is obtained as

$$\sigma_{UC} = \frac{F_{RP}}{A} \tag{5}$$

$$E_{UC} = \frac{\sigma_{UC}}{\varepsilon_{UC}},\ \text{at}\ \varepsilon_{UC} = 0.03 \Rightarrow E_{UC} = \frac{F_{RP}}{0.03A} \tag{6}$$

Where σ_{UC}, F_{RP}, and A denote the stress on the unit cell, the reaction force of the reference point in the displacement of one side of the unit cell, and cross-sectional area of one side of the unit cell, respectively. Furthermore, E_{UC} and ε_{UC} indicate Young's modulus and strain of the unit cell in the elastic limit, correspondingly. This way, the E_{UC} along x-, y-, and z-axes is calculated and the average value of these three results is reported as the final elastic modulus.

To perform the above-mentioned FE modeling, a basic programming language with greater algorithmic ability, such as the C++program, is first used. In this programming language, the position of the reference point and the angle of the centerline of the ESFs relative to the origin of the absolute coordinates are precisely determined. Then, the volume fraction is accurately calculated by considering the imperfect fillers on the sides to establish the periodic boundary conditions. For this purpose, an algorithm is developed and results are inserted into a script file written by the Python programming language. The flowchart of the aforementioned algorithm can be seen in [39]. In the next step, the written Python code is responsible for constructing and dispersing ESFs within the polymers according to the numbers introduced by the C++code. Hence, an ESF with the specified dimensions is formed by Python code and then the ESF is located in the desired space based on the defined positions. Herein, some incomplete or truncated ESFs may place at the corners of the unit cell and the rest of the incomplete ESFs are

Table 1 Dimensions of FE-based unit cells and nanofillers characteristics (ESFs and nanotubes)

SiCNTs		
Chirality	(6,6) armchair	(11,0) zigzag
Length of nanotubes, ESF, and RVEs (L) [Å]	68.06	73.23
MD-based RVEs cross-sectional area [Å^2]	33.61×33.61	35.29×35.29
ESFs diameter [Å]	37.93	39.82
Length of each side of the FE-based unit cell [Å]	451.78	478.21

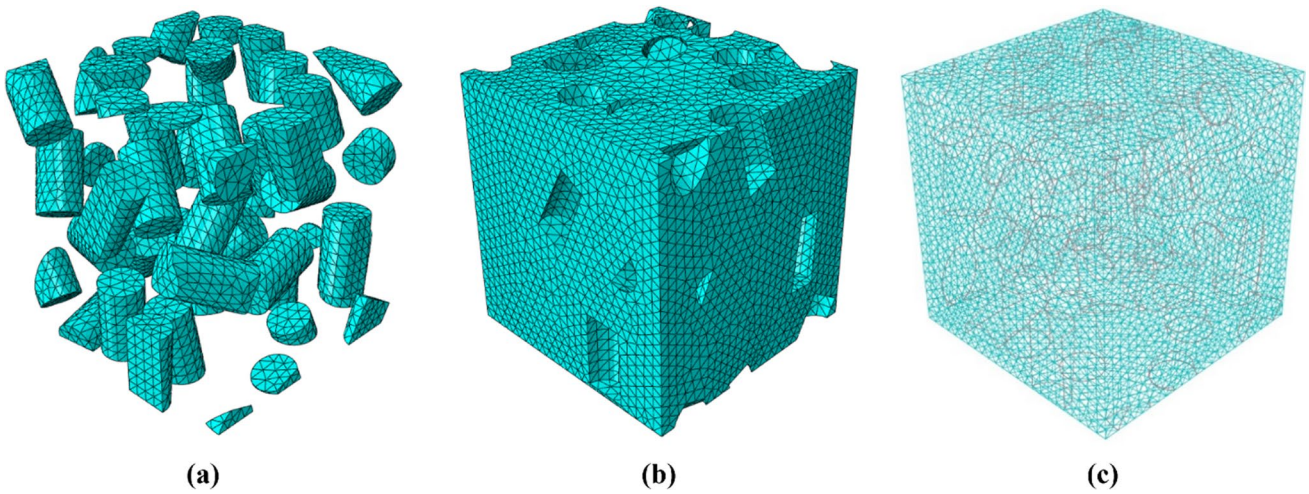

Fig. 6 Meshed structure of the **a** ESFs, **b** polymer matrix, **c** ESFs-SiCNTs/polymer unit cell

utilized in the opposite boundary so that the unit cell possesses a certain number of fillers with the desired volume percentage and the periodicity criterion is satisfied as well. As to the surrounding polymers of the ESFs, a solid cube with the desired dimensions is created and subsequently, the spaces where the ESFs are available in this volume are removed.

3 Results and Discussion

3.1 Elastic Properties of MD-based Nanofillers (SiCNTs and fSiCNTs)

In this section, Young's moduli in longitudinal and transverse directions, as well as shear moduli, are explored in the armchair and zigzag fSiCNTs/polymer RVEs. The findings are compared to the outcomes of the pure SiCNT/polymer. Tables 2–5 are provided to show the list of the results. It has to be pointed out that the actual code has been already validated in our recently published papers [13, 16]. As revealed in Tables 2–5, the longitudinal Young's modulus of the RVEs ($(E_L)E_x$) is extremely larger than transverse Young's modulus ($(E_T)E_y$), and shear moduli (G_{xy} and G_{yz}). This means that the longitudinal Young's modulus affects mechanical properties more significantly compared to the rest of the moduli. Considering the influence of polymer materials, the pure SiCNT/PP RVEs possess a higher stiffness in comparison with the pure SiCNT/PE structures in general. This can be attributed to stronger interactions between the pure SiCNT and the surrounding PP matrix within the interfacial region and larger Young's modulus of the PP compared to the PE [58, 59]. Furthermore, lower values of shear moduli for the pure SiCNT/PE compared to the pure SiCNT/PP imply that their flexibility is smaller than that of the pure SiCNT/PP and thus the required force to laterally deform the pure SiCNT/PE is less than the pure SiCNT/PP. Comparing the pure armchair and zigzag SiCNT/polymer RVEs, the pure zigzag SiCNT/polymer tends to experience higher Young's and shear moduli which means that the pure zigzag SiCNT has a more considerable reinforcing impact. Form Tables 2 and 4, the longitudinal Young's moduli of pure zigzag SiCNT/PE and PP are 8% and 4% greater than those of pure armchair SiCNT/PE and PP, respectively. Moving on to the fSiCNTs/polymer RVEs, the functionalization of the armchair SiCNT causes the longitudinal Young's modulus of the RVE to decrease whereas it often has a beneficial effect on transverse Young's modulus and shear moduli. The reduction of the longitudinal Young's modulus is due to the fundamental alteration of the nanotubes cross-section and hybridization state of atoms, which causes the armchair fSiCNT to show lower resistance to deformation and the RVE strength diminishes in response to the applied tensile load [59, 60]. Regarding the zigzag fSiCNTs/polymer,

Table 2 Young's and shear moduli of the armchair nanotubes/polymers RVEs

Armchair nanotubes/polymers					
Polymers	Nanotubes	Elastic properties (GPa)			
		$E_x(E_L)$	$E_y(E_T)$	G_{xy}	G_{yz}
(PE)	Pure SiCNT	36.35	0.996	0.375	0.409
	F-fSiCNT	32.78	1.003	0.385	0.412
	H-fSiCNT	34.59	0.999	0.379	0.406
	O-fSiCNT	32.23	1.013	0.389	0.423
(PP)	Pure SiCNT	37.44	1.546	0.549	0.562
	F-fSiCNT	33.61	1.552	0.555	0.566
	H-fSiCNT	34.07	1.549	0.551	0.564
	O-fSiCNT	32.27	1.561	0.562	0.568

Table 3 Coefficients of the stiffness matrix (C_{ij}) for the armchair nanotubes/polymers RVEs

Armchair nanotubes/polymers						
Polymers	Nanotubes	Coefficients of the stiffness matrix (GPa)				
		C_{11}	C_{12}	C_{22}	C_{23}	C_{66}
(PE)	Pure SiCNT	36.89	0.674	1.198	0.486	0.375
	F-fSiCNT	33.32	0.680	1.208	0.491	0.385
	H-fSiCNT	35.13	0.677	1.203	0.489	0.379
	O-fSiCNT	32.78	0.678	1.221	0.497	0.389
(PP)	Pure SiCNT	38.17	0.967	1.832	0.711	0.549
	F-fSiCNT	34.35	0.972	1.842	0.717	0.555
	H-fSiCNT	34.81	0.970	1.837	0.715	0.551
	O-fSiCNT	33.01	0.979	1.854	0.722	0.562

the functionalization of the zigzag SiCNT leads the fSiCNTs/PP RVEs to be less stiff compared to the pure zigzag SiCNTs/PP. However, the stiffness of zigzag H- and F-fSiCNTs/PE RVEs is calculated more than that of the pure zigzag SiCNTs/PE. Also, a positive impact can be observed in transverse Young's modulus and shear moduli of the RVEs containing PE when they include the zigzag fSiCNTs (see Table 4). Based on the simulation outcomes, it can be observed that the larger transverse Young's modulus and shear moduli in various directions for the armchair and zigzag O-fSiCNTs/PP compared to the F-fSiCNTs/PP and H-fSiCNTs/PP illustrate that the reinforcement effect of the O-fSiCNTs leads to stiffer configurations and further increased the RVE resistance to transverse deformations. The same results are achieved in the armchair and zigzag O-fSiCNTs/PE in comparison with F-fSiCNTs/PE and H-fSiCNTs/PE peers. In this context, the least strengthening effect on the transverse Young's modulus and shear moduli pertains to the H-fSiCNTs (see Tables 2–5). However, the armchair H-fSiCNTs/polymer show a higher longitudinal Young's modulus as they compare with the outcomes of the armchair O- and F-fSiCNTs/polymer. Similarly, the zigzag H-fSiCNTs/PE is stiffer than that of the zigzag O- and F-fSiCNTs/PE. In the zigzag fSiCNTs/PP, the maximum and minimum stiffness is associated with O- and F-fSiCNTs/PP, and the result of H-fSiCNTs/PP comes in between (see Tables 4 and 5). This can be ascribed to the fact that the highest and lowest effective interfacial areas for interactions in the zigzag O- and F-fSiCNTs/PP are provided, correspondingly. From Tables 2 and 3, the armchair H-fSiCNT has a more profound influence on the longitudinal Young's modulus of RVEs containing the PE compared to the identical system including the PP. However, the armchair F- and O-fSiCNTs exert a more powerful effect on improving the longitudinal Young's modulus of armchair F- and O-fSiCNTs/PP RVEs in comparison with armchair F- and O-fSiCNTs/PE systems. As well as that the transverse Young's modulus and shear moduli of the armchair fSiCNTs/PP RVEs are greater than those of the identical systems including PE. In other words, the ability of the armchair fSiCNTs/PP RVEs to withstand transverse-normal deformations, and shear deformations is more than that of armchair fSiCNTs/PE RVEs. Furthermore, it can be concluded that firstly, the polymer phase compared to the reinforcement has a more key role to play in the determination of transverse Young's modulus and shear moduli of nanocomposite systems. As a result, the values of transverse Young's modulus and shear moduli of the RVEs are close to the quantities of polymers in the absence of nanofillers (pure polymer). Likewise, the zigzag fSiCNTs/PP RVEs can endure higher transverse-normal deformations, and shear deformations compared to the zigzag fSiCNTs/PE system. Moreover, larger effective interplays between two phases in the zigzag F-, O- and H-fSiCNTs/PE RVEs give rise to higher longitudinal Young's moduli than the zigzag F-, O- and H-fSiCNTs/PP, correspondingly (see Table 4 and 5).

3.2 Elastic Properties of MD-based Polymer Matrices (PE and PP)

Elastic properties of pure polymers are required to be determined and fed to ABAQUS software as input data. As mentioned before, the polymers are assumed to be isotropic materials whose properties stay equal in different directions. To prove

Table 4 Young's and shear moduli of the zigzag nanotubes/polymers RVEs

Zigzag nanotubes/polymers					
Polymers	Nanotubes	Elastic properties (GPa)			
		$E_x(E_L)$	$E_y(E_T)$	G_{xy}	G_{yz}
(PE)	Pure SiCNT	39.35	1.007	0.373	0.412
	F-fSiCNT	40.25	1.025	0.386	0.417
	H-fSiCNT	40.77	1.020	0.379	0.411
	O-fSiCNT	39.21	1.042	0.394	0.425
(PP)	Pure SiCNT	39.01	1.557	0.557	0.563
	F-fSiCNT	34.97	1.569	0.558	0.566
	H-fSiCNT	35.31	1.563	0.554	0.560
	O-fSiCNT	38.97	1.572	0.561	0.567

Table 5 Coefficients of the stiffness matrix (C_{ij}) for the zigzag nanotubes/polymers RVEs

Zigzag nanotubes/polymers						
Polymers	Nanotubes	Coefficients of the stiffness matrix (GPa)				
		C_{11}	C_{12}	C_{22}	C_{23}	C_{66}
(PE)	Pure SiCNT	39.89	0.681	1.211	0.491	0.373
	F-fSiCNT	40.80	0.693	1.232	0.500	0.386
	H-fSiCNT	41.32	0.689	1.226	0.497	0.379
	O-fSiCNT	39.77	0.705	1.253	0.509	0.394
(PP)	Pure SiCNT	39.75	0.973	1.844	0.716	0.557
	F-fSiCNT	35.72	0.982	1.866	0.724	0.558
	H-fSiCNT	36.05	0.978	1.854	0.721	0.554
	O-fSiCNT	39.72	0.982	1.861	0.722	0.561

this, the PE and PP with the RVE dimensions are modeled and subjected to tensile and shear loadings. The Young's and shear moduli are measured along x, y, and z directions whose outcomes are approximately equal. The findings demonstrate good agreement with the existing literature and the average of these results is used as the final value (see Table 6). It is found that the PE matrix is less stiff and flexible than the PP matrix.

3.3 Effective Young's Modulus of the ESFs-SiCNTs/polymer Nanocomposite

To validate the code, an RVE containing randomly dispersed pure carbon nanotubes (CNTs) within the PE is simulated. The findings are compared with the Mori–Tanaka approach- and FE-based results in the open literature and also the outcomes based on the proposed method in this paper. For this objective, the armchair CNTs are selected and the volume fraction of the CNTs is accounted for 3% which is equivalent to the ESFs with a volume fraction of 30%. The choice of the CNTs goes back to the fact that first and foremost, the random distribution of the fSiCNTs inside the polymers has not been carried out yet. Secondly, herein, the random dispersion of the fSiCNTs within the polymers is substituted by randomly distributed ESFs comprising the fSiCNTs (ESFs-fSiCNTs). This is considered as one of the innovations of this article and cannot be found in formerly published studies. The results are presented in Table 7 and they agree well with those in the literature. Herein, the $^{E_{UC}}/_{E_P}$ stands for the ratio of effective Young's modulus of the unit cell to Young's modulus of the polymer matrix. Having performed the code verification, the ESFs-armchair fSiCNTs and ESFs-zigzag fSiCNTs at three various volume fractions of 10%, 30%, and 50% are incorporated in the polymers (PE and PP) whose results are given in Figs. 7 and 8. Besides, the findings are compared with those of ESFs-pure SiCNTs/polymer nanocomposite. The simulations illustrated that the functionalization of armchair SiCNTs leads to the reduction of the E_{UC} of the polymer nanocomposite. To put it another way, the use of ESFs-armchair fSiCNTs results in the weakening of the effective elastic modulus of the system. This is due to the reduced longitudinal Young's modulus of the MD-based RVE and this point is elaborated in Section 3.1. In this respect, the least and highest functionalization effect on the decline of effective Young's modulus is related to the ESFs-armchair H-fSiCNTs and ESFs-armchair O-fSiCNTs, respectively. Also, the influence of the ESFs-armchair F-fSiCNTs on diminishing effective Young's modulus lays between them. As can be observed in Fig. 7, the increase of the volume fraction of ESFs-armchair nanotubes has a positive effect on the $^{E_{UC}}/_{E_P}$. As the ESFs' ν_f elevates, the value of the $^{E_{UC}}/_{E_P}$ for the ESFs-pure armchair SiCNTs/PE and ESFs-pure armchair SiCNTs/PP changes from 1.1547 to 1.5017, and 1.1505 to 1.4877, respectively (see Fig. 7). In a defined ESFs' ν_f, the ESFs-pure armchair SiCNTs/PE possesses greater $^{E_{UC}}/_{E_P}$ than that of the ESFs-pure armchair

Table 6 Elastic properties of the pure polymers

Polymers	Elastic properties (GPa)				
	Current research		Previous studies		
	E	*G*	*E*	*G*	*Reference*
(PE)	1.1104	0.4325	1.05	0.38	[61]
(PP)	1.6257	0.5721	1.67	0.6	[62]

Table 7 Results of present research for the ESFs/PE and CNT/PE in comparison with the literature findings

$^{E_{UC}}/_{E_P}$			
Current research		Previous studies [33]	
ESF/PE	CNT/PE	Mori–Tanaka	FEM
1.3013	1.2776	1.23	1.22

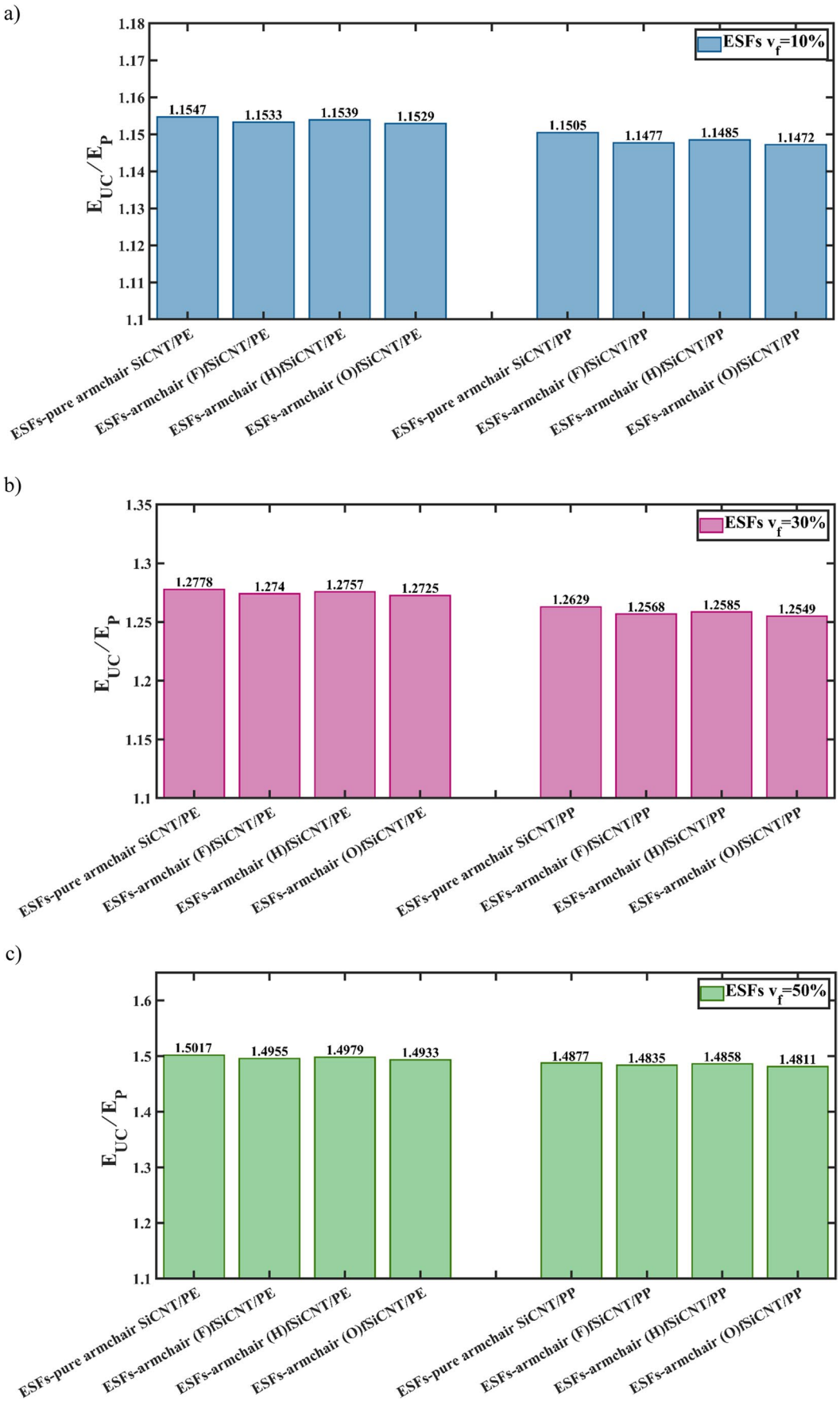

Fig.7 Value of E_{UC}/E_P for the ESFs-armchair nanotubes/polymer at ESFs' ν_f of, **a** 10%, **b** 30%, **c** 50%

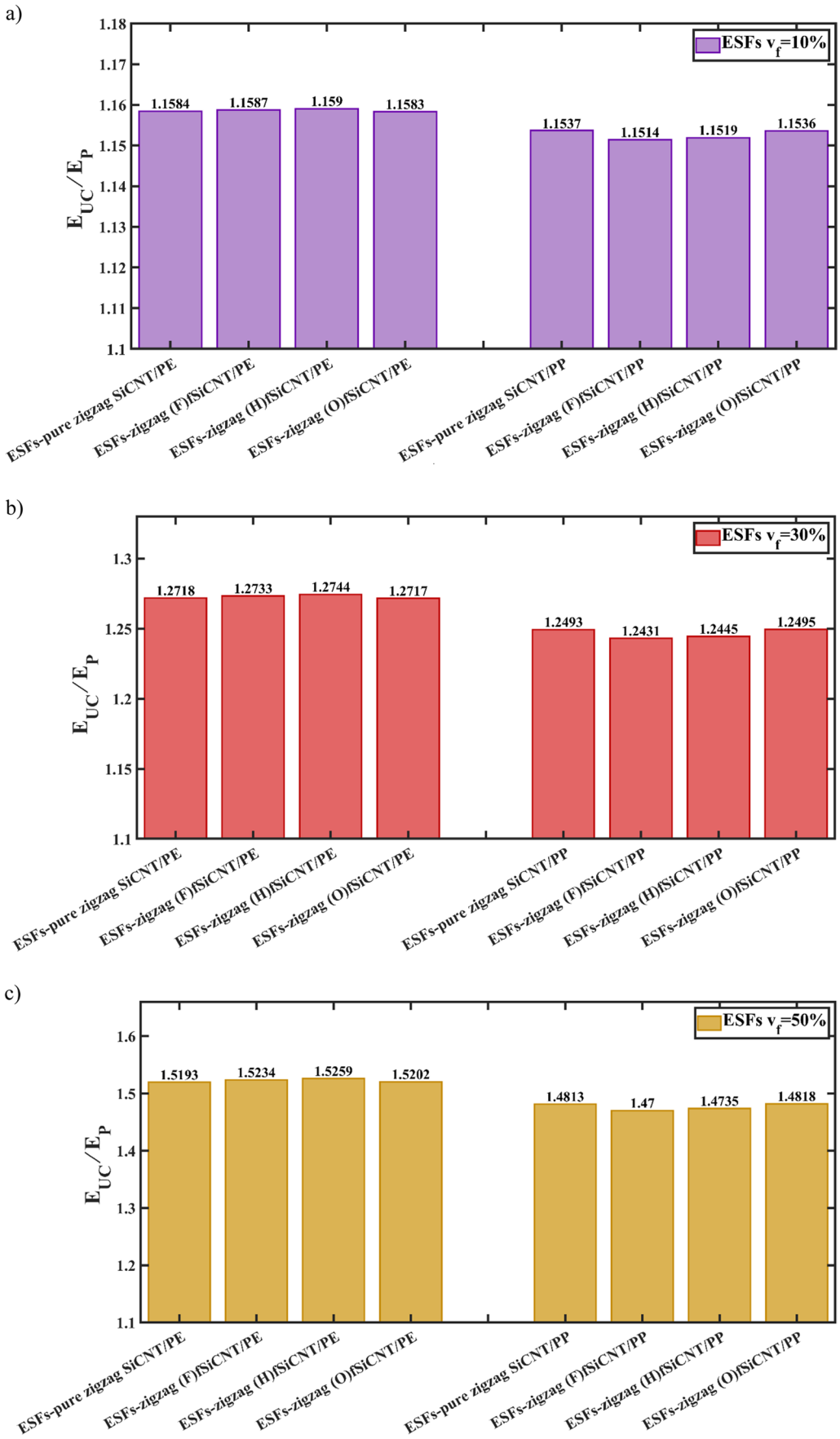

Fig. 8 Value of $^{E_{UC}}/_{E_P}$ for the ESFs-zigzag nanotubes/polymer at ESFs' ν_f of, **a** 10%, **b** 30%, **c** 50%

SiCNTs/PP. This implies that the reinforcing influence of the ESFs-pure armchair SiCNTs on the less stiff polymer (PE) is more notable than that of the PP with higher stiffness. Likewise, the dispersion of ESFs-armchair fSiCNTs within the PE gives rise to a higher effective elastic modulus compared to the ESFs-armchair fSiCNTs intercalated in the PP, and hence the ESFs-armchair fSiCNTs managed to further strengthen the PE. Moving on to Fig. 8, the results demonstrated that the ESFs-pure zigzag SiCNTs/PE are experienced a larger $^{E_{UC}}/_{E_P}$ compared to the ESFs-pure zigzag SiCNTs/PP and the value of $^{E_{UC}}/_{E_P}$ increases by changing ESFs' ν_f from 10 to 50%. These outcomes mean that the higher ESFs' ν_f becomes, the stiffer the polymeric nanocomposite will be. In addition, using the ESFs-pure zigzag SiCNTs could bring further benefits for the PE in comparison with the PP. The $^{E_{UC}}/_{E_P}$ of the ESFs-pure zigzag SiCNTs/PE varies from 1.1584 to 1.5193 whereas the variation range of $^{E_{UC}}/_{E_P}$ for the ESFs-pure zigzag SiCNTs/PP is obtained from 1.1537 to 1.4813 (see Fig. 8). Considering the impact of functional groups (F, H, and O atoms), the higher reactivity of O atom with the PP phase causes the effective elastic modulus of the ESFs-zigzag O-fSiCNTs/PP at 10% ESFs' ν_f is estimated roughly equal to the quantity of the ESFs-pure zigzag SiCNTs/PP. Also, at the ESFs' ν_f over 10%, the effective elastic modulus of the ESFs-zigzag O-fSiCNTs/PP exceeds the ESFs-pure zigzag SiCNTs/PP value which can be attributed to larger interactions energy and more interlocking between the ESFs-zigzag O-fSiCNTs and the PP phase compared to what happens to the ESFs-zigzag F- and H-fSiCNTs and the PP. It can be concluded that the utilization of the randomly dispersed ESFs-zigzag O-fSiCNTs at the volume fractions of 30% or more is in favor of the system stiffness in comparison with the ESFs-pure zigzag SiCNTs/PP. A comparison between the effective elastic modulus of the ESFs-zigzag H- and F-fSiCNTs/PE with the ESFs-pure zigzag SiCNTs/PE reveals that the ESFs-zigzag H- and F-fSiCNTs at all ESFs' ν_f contribute to the stiffness of PE nanocomposites (see Fig. 8). In this regard, the larger longitudinal Young's modulus of the zigzag H- and F-fSiCNTs/PE RVEs than that of their pure counterpart is the most determining factor. It is found that the reinforcing impact of the ESFs-zigzag O-fSiCNTs within the PE is of great importance at the ESFs' ν_f of 50% because of producing a bigger $^{E_{UC}}/_{E_P}$ compared to the ESFs-pure zigzag SiCNTs/PE. However, at the ESFs' ν_f of 10% and 30%, the effect of lower longitudinal Young's modulus of the zigzag O-fSiCNTs/PE RVEs than that of the pure zigzag SiCNTs/PE RVEs dominates the effective elastic modulus of the nanocomposite. From Fig. 8, one can conclude that amongst the ESFs-zigzag fSiCNTs for every ESFs' ν_f, the ESFs-zigzag H-fSiCNTs inserted into the PE are led to higher effective Young's moduli while the maximum effective Young's modulus of PP nanocomposites is achieved in the ESFs-zigzag O-fSiCNTs/PP unit cell.**Fig.7** Value of $^{E_{UC}}/_{E_P}$ for the ESFs-armchair nanotubes/polymer at ESFs' ν_f of, **a** 10%, **b** 30%, **c** 50%**Fig. 8** Value of $^{E_{UC}}/_{E_P}$ for the ESFs-zigzag nanotubes/polymer at ESFs' ν_f of, **a** 10%, **b** 30%, **c** 50%

4 Conclusion

In this paper, a multiscale model was simulated by combining MD and FE approaches. The fundamental objective was to find the effective Young's modulus of polymeric nanocomposites through a two-step simulation. At first, to form the stiffness matrix of the transversely isotropic RVEs, the independent elastic constants were calculated by using MD simulations. Thereupon, the equivalence of the MD-based RVE was modeled via the FE method and the random dispersion of the FE model inside the polymers was conducted. From the simulations, the outcomes could be summarized as follows:

I. Amongst independent elastic characteristics required for the stiffness matrix, the longitudinal Young's modulus was found to be the most efficacious mechanical feature.
II. The longitudinal Young's modulus of pure armchair SiCNTs/polymer and pure zigzag SiCNTs/PP was accounted for larger than that of the armchair fSiCNTs/polymer and zigzag fSiCNTs/PP, respectively.
III. As to the reinforcing effect of armchair fSiCNTs on the longitudinal Young's modulus of the RVEs, the highest and lowest stiffness belonged to the armchair H- and O-fSiCNTs/polymer RVEs, correspondingly. Considering the zigzag fSiCNTs/PE RVEs, similar results were achieved.
IV. The zigzag O- and F-fSiCNTs were affected the maximum and minimum impact on the stiffness of the zigzag fSiCNTs/PP RVEs, respectively.
V. Generally, using the pure zigzag SiCNT and zigzag fSiCNTs instead of their armchair counterparts as reinforcements was led to further enhanced elastic properties of the RVEs.
VI. In every ESFs' ν_f, the use of ESFs-armchair fSiCNTs nanofillers rather than ESFs-pure armchair fSiCNTs resulted in a decline in the $^{E_{UC}}/_{E_P}$. The highest and lowest reduction of the $^{E_{UC}}/_{E_P}$ was associated with the ESFs-armchair O- and H-fSiCNTs/polymer, correspondingly.
VII. In each ESFs' ν_f, the value of $^{E_{UC}}/_{E_P}$ for the ESFs-armchair and zigzag fSiCNTs/PE was computed more than that of the ESFs-armchair and zigzag fSiCNTs/PP which demonstrated that the reinforcement effect of the ESFs-armchair and zigzag fSiCNTs on the PE was more remarkable.

VIII. The random dispersion of the ESFs-zigzag H- and F-fSiCNTs within the PP instead of the ESFs-pure zigzag SiCNTs diminished the $^{E_{UC}}/_{E_P}$ while at the ESFs' ν_f over 10%, the randomly distributed ESFs-zigzag O-fSiCNTs inside the PP enhanced the $^{E_{UC}}/_{E_P}$.

IX. Incorporation of the ESFs-zigzag H- and F-fSiCNTs into the PE rather than using the ESFs-pure zigzag SiCNTs was led to the elevated effective elastic modulus. However, just at the ESFs' ν_f of 50%, the ESFs-zigzag O-fSiCNTs/PE was experienced a larger $^{E_{UC}}/_{E_P}$ compared to that of the ESFs-pure zigzag SiCNTs/PE.

Acknowledgements We are grateful to all the people who helped us advance science so that we could do this research.

Authors' contributions **M. Eghbalian:** Conceptualization, Methodology, Software, Investigation.

R. Ansari: Supervision, Conceptualization, Writing- Reviewing and Editing.

S. Haghighi: Methodology, Software, Writing- Original draft preparation.

Funding Declaration of competing interest the authors declare that they have no known competing financial interests or personal relationships that could have appeared to influence the work reported in this paper.

Data Availability

• The raw/processed data required to reproduce these findings cannot be shared at this time due to legal or ethical reasons.

• The raw/processed data required to reproduce these findings cannot be shared at this time as the data also forms part of an ongoing study.

The raw/processed data required to reproduce these findings cannot be shared at this time due to technical or time limitations.

Code Availability The code required to reproduce these findings cannot be shared at this time due to technical or time limitations.

Declarations

Ethics Approval N/A.

Consent to Participate N/A.

Consent for Publication N/A.

Competing interests The authors declare no competing interests.

References

1. Benzait Z, Trabzon L (2018) A review of recent research on materials used in polymer–matrix composites for body armor application. J Compos Mater 52(23):3241–3263
2. Gopanna A, Rajan KP, Thomas SP, Chavali M (2019) Polyethylene and polypropylene matrix composites for biomedical applications, Chapter 6-Materials for Biomedical Engineering. Elsevier, pp 175–216
3. Trinh SN, Sastry S (2016) Processing and properties of metal matrix composites, Mechanical Engineering and Materials Science Independent Study, p 10
4. Haghighi S, Ansari R, Ajori S (2020) A molecular dynamics study on the interfacial properties of carbene-functionalized graphene/polymer nanocomposites. Int J Mech Mater Des 16:387–400
5. Eghbalian M, Ansari R, Rouhi S (2021) Effects of geometrical parameters and functionalization percentage on the mechanical properties of oxygenated single-walled carbon nanotubes. J Mol Model 27(12):1–17
6. Dang Z-M, Yuan J-K, Zha J-W, Zhou T, Li S-T, Hu G-H (2012) Fundamentals, processes and applications of high-permittivity polymer–matrix composites. Prog Mater Sci 57(4):660–723
7. Krishnaraj V, Zitoune R, Davim JP (2013) Drilling of polymer-matrix composites, vol 13. Springer, Heidelberg
8. Haghighi S, Ansari R, Ajori S (2019) Influence of polyethylene cross-linked functionalization on the interfacial properties of carbon nanotube-reinforced polymer nanocomposites: a molecular dynamics study. J Mol Model 25(4):1–13
9. Ansari R, Rouhi S, Eghbalian M (2017) On the elastic properties of curved carbon nanotubes/polymer nanocomposites: A modified rule of mixture. J Reinf Plast Compos 36(14):991–1008
10. Jawalkar C, Verma AS, Suri N (2017) Fabrication of aluminium metal matrix composites with particulate reinforcement: a review. Mater Today Proc 4(2):2927–2936
11. Mangalgiri P (2005) Polymer-matrix composites for high-temperature applications. Def Sci J 55(2):175
12. Skoczylas J, Samborski S, Kłonica M (2019) The application of composite materials in the aerospace industry. J Technol Exploit Mech Eng 5(1):1–6
13. Eghbalian M, Ansari R, Haghighi S (2022) Molecular dynamics study of mechanical properties and fracture behavior of carbon and silicon carbide nanotubes under chemical adsorption of atoms. Diam Relat Mater 121:108764
14. Kohestanian M, Sohbatzadeh Z, Rezaee S (2020) Mechanical properties of continuous fiber composites of cubic silicon carbide (3C-SiC)/different types of carbon nanotubes (SWCNTs, RSWCNTs, and MWCNTs): A molecular dynamics simulation. Mater Today Commun 23:100922
15. Setoodeh A, Jahanshahi M, Attariani H (2009) Atomistic simulations of the buckling behavior of perfect and defective silicon carbide nanotubes. Comput Mater Sci 47(2):388–397
16. Eghbalian M, Ansari R, Haghighi S (2021) On the mechanical properties and fracture analysis of polymer nanocomposites reinforced by functionalized silicon carbide nanotubes: a molecular dynamics investigation. J Mol Graph Model 111:108086
17. Pan H, Si X (2009) Molecular dynamics simulations of diameter dependence tensile behavior of silicon carbide nanotubes. Physica B 404(12–13):1809–1812
18. Memarian F, Fereidoon A, Khodaei S, Mashhadzadeh AH, Ganji MD (2017) Molecular dynamic study of mechanical properties of single/double wall SiCNTs: Consideration temperature, diameter and interlayer distance. Vacuum 139:93–100
19. Dong X, Shin YC (2017) Multi-scale modeling of thermal conductivity of SiC-reinforced aluminum metal matrix composite. J Compos Mater 51(28):3941–3953
20. Khatti Z, Hashemianzadeh SM, Shafiei SA (2018) A molecular study on drug delivery system based on carbon nanotube compared to silicon carbide nanotube for encapsulation of platinum-based anticancer drug. Adv Pharm Bull 8(1):163
21. Eghbalian M, Ansari R, Rouhi S (2021) Mechanical properties of oxygen-functionalized silicon carbide nanotubes: A molecular dynamics study. Physica B 610:412939
22. Zhang Y, Huang H (2008) Stability of single-wall silicon carbide nanotubes–molecular dynamics simulations. Comput Mater Sci 43(4):664–669
23. Bai D (2011) Size, morphology and temperature dependence of the thermal conductivity of single-walled silicon carbide nanotubes. Fullerenes, Nanotubes, Carbon Nanostruct 19(4):271–288

24. Borowiak-Palen E et al (2005) Bulk synthesis of carbon-filled silicon carbide nanotubes with a narrow diameter distribution. J Appl Phys 97:056102
25. Mercan K, Civalek Ö (2017) Buckling analysis of Silicon carbide nanotubes (SiCNTs) with surface effect and nonlocal elasticity using the method of HDQ. Compos B Eng 114:34–45
26. Mercan K (2019) Comparative Stability Analysis of Silicone Carbide Nanotube using MD Simulation and FEM Software. Int J Eng Appl Sci 11(4):507–511
27. Sheng-Jie W, Chun-Lai Z, Zhi-Guo W (2010) Melting of single-walled silicon carbide nanotubes: density functional molecular dynamics simulation. Chin Phys Lett 27(10):106101
28. Mpourmpakis G, Froudakis GE, Lithoxoos GP, Samios J (2006) SiC nanotubes: a novel material for hydrogen storage. Nano Lett 6(8):1581–1583
29. Miyamoto Y, Yu BD (2002) Computational designing of graphitic silicon carbide and its tubular forms. Appl Phys Lett 80(4):586–588
30. Cao F, Xu X, Ren W, Zhao C (2010) Theoretical study of O2 molecular adsorption and dissociation on silicon carbide nanotubes. J Phys Chem C 114(2):970–976
31. Taguchi T, Igawa N, Yamamoto H, Jitsukawa S (2005) Synthesis of silicon carbide nanotubes. J Am Ceram Soc 88(2):459–461
32. Sun X-H et al (2002) Formation of silicon carbide nanotubes and nanowires via reaction of silicon (from disproportionation of silicon monoxide) with carbon nanotubes. J Am Chem Soc 124(48):14464–14471
33. Mortazavi B, Baniassadi M, Bardon J, Ahzi S (2013) Modeling of two-phase random composite materials by finite element, Mori-Tanaka and strong contrast methods. Compos B Eng 45(1):1117–1125
34. Eghbalian M, Ansari R, Haghighi S (2022) A combined molecular dynamics-finite element multiscale modeling to analyze the mechanical properties of randomly dispersed, chemisorbed carbon nanotubes/polymer nanocomposites. Mech Adv Mater Struct 1–17
35. Chandra Y, Scarpa F, Chowdhury R, Adhikari S, Sienz J (2013) Multiscale hybrid atomistic-FE approach for the nonlinear tensile behaviour of graphene nanocomposites. Compos A Appl Sci Manuf 46:147–153
36. Doagou-Rad S, Jensen J, Islam A, Mishnaevsky L Jr (2019) Multiscale molecular dynamics-FE modeling of polymeric nanocomposites reinforced with carbon nanotubes and graphene. Compos Struct 217:27–36
37. Atescan Y, Hadden CM, Wardle BL, Odegard GM, Cebeci H (2015) Molecular Dynamics and Finite Element Investigation of Polymer Interphase Effects on Effective Stiffness of Wavy Aligned Carbon Nanotube Composites, in 56th AIAA/ASCE/AHS/ASC Structures, Structural Dynamics, and Materials Conference, p. 0701
38. Eyvazian A, Zhang C, Musharavati F, Farazin A, Mohammadimehr M, Khan A (2021) Effects of appearance characteristics on the mechanical properties of defective SWCNTs: using finite element methods and molecular dynamics simulation. Eur Phys J Plus 136(9):1–24
39. Khani N, Yildiz M, Koc B (2016) Elastic properties of coiled carbon nanotube reinforced nanocomposite: A finite element study. Mater Des 109:123–132
40. Eghbalian M, Ansari R, Haghighi S (2023) Molecular dynamics investigation of the mechanical properties and fracture behaviour of hydroxyl-functionalised carbon and silicon carbide nanotubes-reinforced polymer nanocomposites. Mol Simul 1–12
41. Chen X, Alian A, Meguid S (2019) Modeling of CNT-reinforced nanocomposite with complex morphologies using modified embedded finite element technique. Compos Struct 227:111329
42. Poorsolhjouy A, Hassan Naei M (2015) Effects of carbon nanotubes' dispersion on effective mechanical properties of nanocomposites: A finite element study. J Reinf Plast Compos. 34(16):1315–1328
43. Lu X, Zhang A, Dubrunfaut O, He D, Pichon L, Bai J (2020) Numerical modeling and experimental characterization of the AC conductivity and dielectric properties of CNT/polymer nanocomposites. Compos Sci Technol 194:108150
44. Charitos I, Drougkas A, Kontou E (2020) Prediction of the elastic modulus of LLDPE/CNT nanocomposites by analytical modeling and finite element analysis. Mater Today Commun 24:101070
45. Tserpes K, Chanteli A (2013) Parametric numerical evaluation of the effective elastic properties of carbon nanotube-reinforced polymers. Compos Struct 99:366–374
46. Kassa MK, Arumugam AB (2020) Micromechanical modeling and characterization of elastic behavior of carbon nanotube-reinforced polymer nanocomposites: A combined numerical approach and experimental verification. Polym Compos 41(8):3322–3339
47. Eghbalian M, Ansari R, Bidgoli MO, Rouhi S (2022) Finite element investigation of the geometrical parameters of waviness carbon nanotube on directional young's and shear elastic modulus of polymer nanocomposites. J Inst Eng (India): Series D 1–14
48. Chwał M, Muc A (2016) Transversely isotropic properties of carbon nanotube/polymer composites. Compos B Eng 88:295–300
49. Mayo SL, Olafson BD, Goddard WA (1990) DREIDING: a generic force field for molecular simulations. J Phys Chem 94(26):8897–8909
50. Tersoff J (1988) New empirical approach for the structure and energy of covalent systems. Phys Rev B 37(12):6991
51. Allen MP, Tildesley DJ (2017) Computer simulation of liquids. Oxford University Press
52. Ajori S, Haghighi S, Ansari R (2017) Buckling behavior of carbon nanotubes functionalized with carbene under physical adsorption of polymer chains: a molecular dynamics study. Braz J Phys 47(6):606–616
53. Hoover WG (1985) Canonical dynamics: Equilibrium phase-space distributions. Phys Rev A 31(3):1695
54. Anjana R, Sharma S, Bansal A (2016) Molecular dynamics simulation of carbon nanotube reinforced polyethylene composites. J Compos Mater 0021998316674264(0):(0)
55. Bhaskar P, Mohamed RH (2012) Analytical estimation of elastic properties of polypropylene fiber matrix composite by finite element analysis. Adv Mater Phys Chem 2(1):23–30
56. Shingare K, Gupta M, Kundalwal S (2020) Evaluation of effective properties for smart graphene reinforced nanocomposite materials. Mater Today Proc 23:523–527
57. Martínez L, Andrade R, Birgin EG, Martínez JM (2009) PACKMOL: A package for building initial configurations for molecular dynamics simulations. J Comput Chem 30(13):2157–2164
58. Lu J, Luo M, Yakobson BI (2018) Glass composites reinforced with silicon-doped carbon nanotubes. Carbon 128:231–236
59. Bansal SA, Singh AP, Singh S, Kumar S (2023) Bisphenol-a–carbon nanotube nanocomposite: interfacial DFT prediction and experimental strength testing. Langmuir
60. Tsafack T, Alred JM, Wise KE, Jensen B, Siochi E, Yakobson BI (2016) Exploring the interface between single-walled carbon nanotubes and epoxy resin. Carbon 105:600–606
61. Rouhi S, Alizadeh Y, Ansari R, Aryayi M (2015) Using molecular dynamics simulations and finite element method to study the mechanical properties of nanotube reinforced polyethylene and polyketone. Mod Phys Lett B 29(26):1550155
62. Yang S, Yu S, Kyoung W, Han D-S, Cho M (2012) Multiscale modeling of size-dependent elastic properties of carbon nanotube/polymer nanocomposites with interfacial imperfections. Polymer 53(2):623–633